Chemical Science

ROYAL SOCIETY OF CHEMISTRY

EDGE ARTICLE

View Article Online
View Journal | View Issue

Cite this: *Chem. Sci.*, 2025, **16**, 15602

All publication charges for this article have been paid for by the Royal Society of Chemistry

Special solvation effects of mixed water and alcohols revealed by molecular aggregation†

Linghao Meng,‡ Rong Wei,‡ Zhaoxin Xie, ‡ Di Zhang, * Xiaohan Wan, Han Han, Wenjing Shi, Ziqi Zhu, Xiao Xiao, Yi Qin Gao * and Dahui Zhao *

Received 18th May 2025
Accepted 21st July 2025

DOI: 10.1039/d5sc03588k

rsc.li/chemical-science

Owing to their green nature, good miscibility and tunable polarity, alcohols are widely used as popular co-solvents of water in supramolecular assembly. Intriguingly, the solvation properties of water/alcohol mixtures often show a complex dependence on the composition. Herein, the unusual solvation effects of water and alcohol mixtures are elucidated by examining the aggregation motif changes of amphiphilic polycycles bearing more polar side chains. While the molecule assembles into long fibrous J-aggregates in pure water and alcohols, H-aggregates of smaller sizes appear in water–alcohol mixtures. Similar dissociation is found to occur in different low-carbon alcohol–water systems, but H/J switching takes place at different volume ratios, depending on the alcohol structure. It is thus speculated that the aggregate dissociations reflect an enhanced solubilizing ability of the mixed solvents, which is assumed to be related to the microscopic structures of the water–alcohol binary systems. That is, the highly structured networks formed by mixed water and alcohols possess enhanced solvating capacity for the amphiphilic molecules, and alcohols having longer alkyl groups and forming larger structured hydration shells in water disrupt the aggregation more effectively. Molecular dynamics simulations have provided supportive evidence for the special solubilizing properties of mixed water and alcohols.

Introduction

Polycyclic aromatic molecules with extended π-scaffolds have vast potential in various fields, such as organic electronics[1–4] and biomedical technologies.[5,6] The supramolecular behaviour of pertinent systems is recognized to have profound influence on functional properties, and thus gaining better control over the molecular aggregation processes is important to their applications. Solvent is apparently among the pivotal factors that govern the molecular assembly behavior during solution processing,[7,8] and it induces diverse solvent-dependent characteristics, including morphology,[9–15] assembly energetics,[16–18] and supramolecular chirality,[19–21] with various conjugated molecules.[22] Additionally, the introduction of solvent mixtures may confer additional complexity to the aggregation properties of supramolecular systems, which is particularly evident when pronounced secondary interactions exist with the solute, aggregates and solvent molecules. Recently, an increasing number of studies have been reported pertinent to the influences of mixed solvents over supramolecular aggregation behaviours, including the pathway selection, aggregation kinetics, and more.[23–27] Hence, an in-depth understanding of the solvent effects is indispensable to the solution processing of soft materials.

Among all different solvents, water is undoubtedly the most attractive processing medium due to its ultimate eco-friendly nature.[28–37] Nonetheless, the intense hydrophobic effects experienced by organic molecules in water often lead to undesirable assembly dynamics and difficulties with supramolecular manipulations.[38–41] To modulate the hydrophobic force, co-solvents are widely employed. Among all miscible solvents, assorted alcohols are particularly appealing due to their hydrogen-bonding capability and tunable polarity. Nonetheless, mixed solvents have been repeatedly reported to entail unexpected complexity.[23] For instance, Meijer and Palmans *et al.* discovered a discotic organic amphiphile to manifest three different helically bundled structures in binary water–isopropanol (IPA) solvents ranging from low to high IPA content.[42] In particular, aggregates of a lower aspect ratio were observed in the medium IPA regime. More recently, Rao and coworkers reported a supramolecular depolymerization process effected by mixed water–IPA.[43] In this case, an aromatic molecule bearing cationic side chains adopted the aggregated state in both water and high IPA-content solvents but dissociated to monomers at more balanced IPA–water volume ratios. These studies unveiled pronounced nonlinear dependence of solvation properties on the solvent composition, but whether such unusual behaviors

Beijing National Laboratory for Molecular Sciences, Centre for the Soft Matter Science and Engineering, The Key Laboratory of Polymer Chemistry and Physics of the Ministry of Education, College of Chemistry, Peking University, Beijing 100871, China. E-mail: dizhang@pku.edu.cn; gaoyq@pku.edu.cn; dhzhao@pku.edu.cn

† Electronic supplementary information (ESI) available. See DOI: https://doi.org/10.1039/d5sc03588k

‡ These authors contributed equally to this work.

are unique to the IPA or common to alternative alcohols and the underlying reasons still await further research.

In our previous work, we studied the self-aggregation of a polycyclic aromatic dicarboximide bearing alkyl side chains (Fig. 1).[44–46] This molecule was found to be able to assume two different aggregation motifs (H and J) in aliphatic solvents. Because the H-type structure features the anti-cooperative propagating energetics and the J-species exhibit a cooperative growing mechanism, their energy profiles show contrasting dependency on the degree of polymerization, leading to a crossover at a certain point (Fig. 1a). Hence, the H-aggregates are manifested as smaller oligomers when the molecular association strength is low to moderate, whereas J-aggregates emerge only if the driving force for molecular packing is sufficient for promoting high polymer formation. Both the H- and J-aggregates are thermodynamically stable species but appear with different degrees of molecular aggregation. By virtue of the distinct photophysical characteristics of H- and J-aggregates, the molecule uniquely displayed easily distinguishable spectral signatures, allowing for easy differentiation and identification of the smaller and larger supramolecular aggregates.

Taking advantage of this property, in the current contribution, we have modified the side chains of the molecule from aliphatic groups to aliphatic-spacer tethered tri(ethylene glycol) methyl ethers (triglyme), while keeping the aromatic skeleton unchanged (Fig. 1c), such that the aggregation behaviors in aliphatic solvents can be replicated under aqueous conditions. As expected, the J-aggregates are well reproduced by molecule **1** in water and various low-carbon alcohols, as evidenced by the appearance of a J-band nearly identical to that observed in nonpolar solutions. The appearance of J-aggregates proves that water and alcohols can provide ample solvophobic driving force for molecule **1** to form supramolecular high polymers. More interestingly, when water is mixed with an alcohol at certain volume ratios, the J-aggregates are found to transform to H-aggregates. As the H-aggregates are recognized to be of lower degrees of association, such a transition unambiguously signifies mitigated solvophobicity of the binary solvents to the amphiphiles, as compared to pure water and pure alcohols. By monitoring the H–J interconversion in a series of binary aqueous solvents containing different alcohols (methanol, ethanol, *n*- and *i*-propanol), the solvation effects of the mixed solvents are systematically examined (Fig. 1c). The findings here echo the results from a previous investigation using NMR spectroscopy,[47] which uncovered the non-homogeneous microstructures of water–alcohol mixtures. Our study further elucidates that the binary solvents may solvate the amphiphilic solute more effectively than pure water and alcohols, and aqueous solvents composed of assorted alcohols impart different solvation and solvophobicity properties. The current work also offers a unique example, demonstrating the values of supramolecular systems in serving as sensitive gauges for assessing solvent properties.

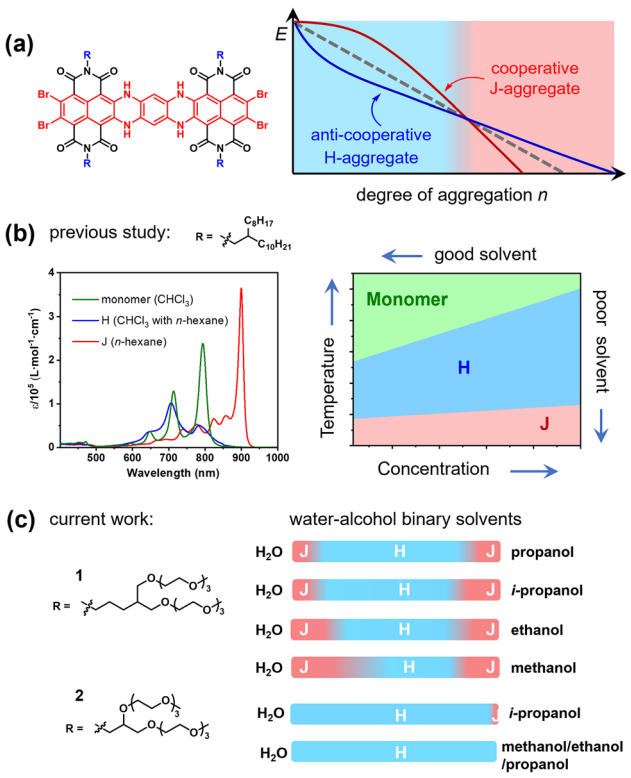

Fig. 1 (a) Schematic energy profiles of competing anti-cooperative H- (blue) and cooperative J-aggregation (red) paths, showing different dependency on the degree of aggregation; (b) absorption spectra of a previously studied analogue having alkyl side chains in good ($CHCl_3$), poor (*n*-hexane, favouring J), and mixed (promoting H) solvents, with a qualitative diagram depicting the transitions among monomer, H- and J-aggregates; (c) binary solvent (water mixed with varied alcohols) composition ranges promoting H- or J-aggregates of amphiphiles **1** and **2**.

Results

Syntheses

Compounds **1** and **2** are synthesized *via* procedures modified from those used for preparing alkyl-substituted analogues.[44]

The imidation of tetrabromonaphthalene dianhydride[44,48] is conducted with two different alkyl amines appended with triglyme groups at varied branch positions to afford naphthalenediimides **3a** and **3b**, which then undergo nucleophilic substitution by benzene-1,2,4,5-tetraamine (TAP) to generate amphiphiles **1** and **2** in 45% and 35% yields, respectively (Scheme 1).

Aggregation in pure solvents

The absorption spectra of **1** are first collected in various pure solvents (Fig. S1†). As a good solvent, chloroform produces a solution of **1** in its monomer state, with the absorption spectrum showing well resolved vibronic peaks and the 0–0 transition at 794 nm. In alternative media that presumably solvate the triglyme side chains better than the aromatic framework, aggregation occurs to varied degrees. In tetrahydrofuran (THF) and acetonitrile (ACN), H-aggregates are formed, as evidenced by the reduced intensity of the 0–0 peak. In contrast, a significantly red-shifted J-band with a narrower FWHM than that of the 0–0 transition is detected at 905 nm in

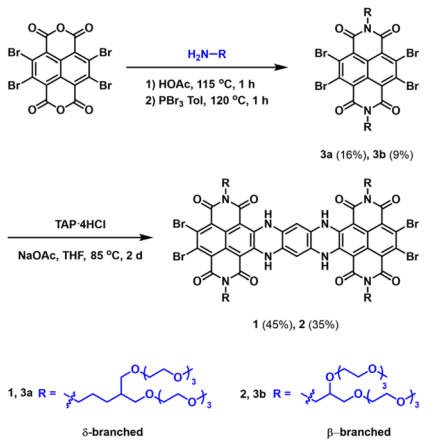

Scheme 1 Syntheses of amphiphiles **1** and **2**.

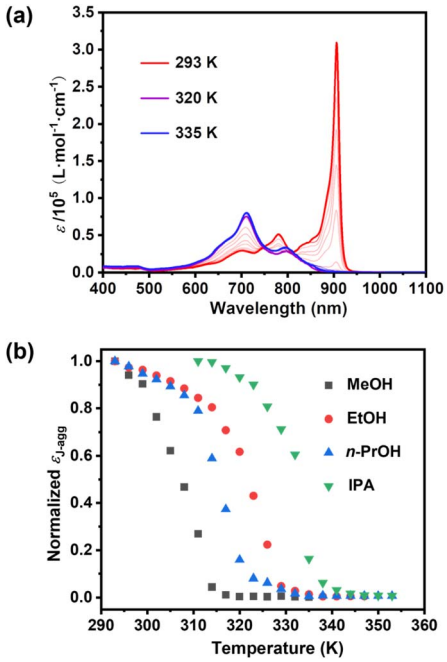

Fig. 2 (a) Absorption spectra of **1** (3.0×10^{-6} M) in methanol at varied temperatures, showing transition from J- to H-aggregates upon heating; (b) thermal dissociations of J-aggregates of **1** in different alcohols (all at 3.0×10^{-6} M).

water and various alcohols, including methanol, ethanol, and *n*-propanol.[44,45] In IPA, the J-band is slightly broadened on the long-wavelength side, suggesting more delocalized excitons, likely from more extended superstructures with certain longer-range disorder in this alcohol solvent. Basically, J-aggregates are unambiguously identified with **1** in more polar solvents, including water and four alcohol solvents. The aggregation behaviors in mixed IPA–$CHCl_3$ are then examined, and it is found that while J-aggregates are formed under highly IPA-rich conditions, they gradually transform to H-aggregates when the $CHCl_3$ content is increased to *ca.* 10 vol%. With continually increased $CHCl_3$, the H-aggregates are degraded to monomers (Fig. S9†). These observations indicate that the aggregation behaviors of **1** are very similar to those of its analogue having alkyl side chains (Fig. 1b), which have been investigated earlier.[44,45] That is, its H-aggregates are smaller oligomers formed in the presence of medium aggregation driving force, *e.g.*, by mixing the good and poor solvents, whilst the J-species are larger aggregates, driven by stronger π–π stacking interactions of solvophobic nature.

Next, the thermal stability of the J-aggregates in these solvents is examined. In methanol, ethanol and *n*-propanol, the J-band attenuates consistently with increasing temperature, reflecting the thermal dissociation of the J-aggregates (Fig. 2a and S2†). When the IPA solution is heated, the J-band first turns slightly narrower with a small hypsochromic shift, becoming identical to those shown in the other three alcohol solutions. This observation further confirms that the minor J-band broadening originates from larger aggregates in IPA. At above 310 K, the J-band also starts to decrease in IPA. When plotting the J-band intensity changes against the temperature, non-sigmoidal curves indicative of cooperative assembling processes are depicted by all four alcohol solutions. Moreover, when the J-band vanishes, the absorption spectra all become assignable to H-aggregates. Evidently, similar to the aliphatic side-chain analogue,[45] the larger J-aggregates formed in the alcohol solutions first degrade to smaller H-type species at elevated temperatures before they completely dissociate into monomers. Moreover, the temperature-dependent behaviors reveal that the thermal stability of the J-aggregates differs in the four alcohols (Fig. 2b), with the IPA solution showing the highest J-to-H transition temperature, followed by ethanol and *n*-propanol; the poorest thermal stability is observed in methanol. No clear correlation can be drawn between the relative thermal stability of the J-aggregate and the structure or polarity of the alcohol molecules, and the reason is unclear at this point.

Unlike in alcohols, the J-aggregation of **1** in water manifests a thermally induced enhancement, resulting in precipitation at elevated temperature. That is, when an aqueous solution of **1** is heated, the J-band maintains its intensity without obvious falling until 323 K, above which precipitation is observed (Fig. S3†). Such thermal behaviors indicate that J-aggregation in water features an entropy-driven mechanism, which is relatively common for organic supramolecular systems in water-rich solvents.

Compared with **1**, molecule **2** has the same polycyclic aromatic skeleton, but the branch point for anchoring the two triglyme side groups is installed closer to the imide nitrogen, *i.e.*, from δ- to β-carbon (Scheme 1). Hence, when these triglyme chains are similarly solvated, greater steric repulsions are expected with **2** compared to **1**, thereby hindering the intermolecular stacking among the aromatic cores and leading to weakened aggregation ability of **2**. As anticipated, instead of J-aggregates, molecule **2** only forms smaller H-oligomers in methanol and *n*-propanol. In ethanol, J-aggregates are observed only at increased concentrations, which co-exist with dominant H- species, and such J-aggregates are rather labile, and readily degraded to smaller H-aggregates upon slight dilution or heating (Fig. S16†). Only in IPA, **2** is able to form J-aggregates

completely, and upon heating, these J-aggregates are as well transformed to H-species (Fig. S15†). Upon reducing the concentration or raising the temperature, the H-aggregates of **2** show slight tendency of degradation (to monomers), further proving its weakened aggregation ability. All these phenomena not only confirm that among the four alcohols, IPA is the most potent solvent for promoting J-aggregation of triglyme-decorated amphiphiles, and more importantly, the weakened J-aggregation capability of **2** relative to **1** clearly reveals that the aggregate sizes, which are reflected by the association motif changes in the form of H- and J-aggregates, are influenced by the extent of solvation experienced by the side chains.

Additionally, the absorption spectroscopy also indicates that the H-aggregates are formed by **2** in water at room temperature, but they transform to the J-form at increased temperatures (Fig. S15†). This observation verifies the entropy-favored nature of aggregation in water. Apparently, the ability to form larger J-aggregates is tempered by the greater steric hindrance presented by the side chains in molecule **2**. Only when the driving force for the aromatic stack is enhanced, *e.g.*, by raising the concentration in IPA or increasing temperature in water, larger J-species may emerge. All these results reinforce the notion that with amphiphiles **1** and **2**, their degrees of aggregation, as well as the appearance of H or J motifs, are influenced by the steric conditions around the side chains, which may be modulated by modifying the structures or tuning the solvation properties.

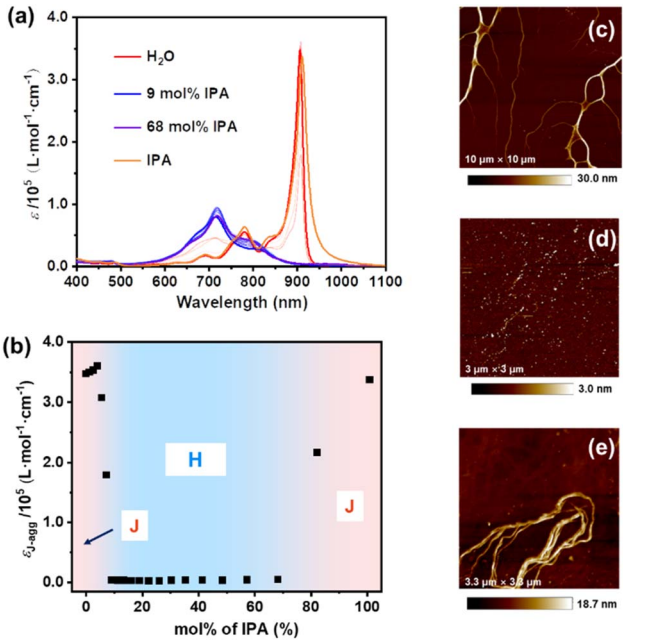

Fig. 3 (a) Absorption spectra of **1** (3.0×10^{-6} M) and (b) corresponding extinction coefficient change of J-bands with solvent components at room temperature; AFM height images on silicon from drop-cast solutions of **1** (3.0×10^{-6} M) in (c) IPA, (d) water–IPA (19 mol%), and (e) water.

Aggregation in solvent mixtures

From the above results, it is clear that the four examined alcohols and water are all suitable solvents for promoting the J-aggregation of **1**, presumably by solvating the triglyme groups while imposing hydrophobic force to drive the packing of the aromatic moiety and short aliphatic linkers. Then, the assembling behaviors of **1** in binary water–alcohol solvents are investigated and unexpected results ensue. First, molecule **1** is dispersed into a series of binary solvents with mixed IPA and water at varied volume ratios. Although J-aggregates are still observed when either water or IPA constitutes the dominant component of the binary solvent, the absorption spectra become unambiguously ascribable to H-aggregates when IPA appears in a medium range of *ca.* 9 to 68 mole percent (mol%) (Fig. 3). This mixed-solvent-induced J- to H-aggregate transition and degradation process is found to be marginally concentration-dependent, since the composition range that produces the H-aggregate is only narrowed slightly with a highly concentrated solution (Fig. S5†). Basically, the mixed IPA–water solvents appear to induce a partial aggregate dissociation, as evidenced by a motif transition from J to H.

Atomic force microscopy (AFM) further evidences the aggregation motif change taking place with **1** in the mixed solvents (Fig. 3). Solution-cast samples from both pure IPA and water depict long fibrous structures, whereas much smaller globules of irregular shapes are exhibited by mixed water–IPA solutions. Such two types of morphological features are nearly identical to those of previously observed J- and H-aggregates that are formed by the alkyl-substituted analogue. Moreover, the dynamic light scattering (DLS) technique also confirms that the J-aggregates formed in IPA are much larger in size than the H-aggregates detected in mixed IPA–water solvents (Fig. S6†), while the aggregates found in water presumably have even larger sizes because they could not be determined with DLS for exceeding the detection limit of the instrument. All these characterization results substantiate the conclusion that the larger J-aggregates formed in pure and highly water- or IPA-rich solvents are disrupted into smaller H-aggregates in solutions with more balanced water–IPA ratios.

Next, the thermal properties of the J-aggregates in mixed alcohol–water solvents are examined. By following the J-band intensity changes with temperature in solvents of different IPA–water ratios, a unique trend is observed with the J- to H-aggregate (degradation) transition temperature in terms of its dependency on the solvent content, which evidently implies a nonlinear variation of the solvation properties with the solvent composition (Fig. 4). In particular, by following the J-band intensity changes with temperature (Fig. 4a), the H–J transition temperatures in solvents of lower (5, 6 & 7 mol%) and higher (88 mol% and pure) IPA contents are determined (Fig. 4b). When the transition temperatures are plotted against the solvent composition (Fig. 4c), it is clearly seen that the J-aggregates manifest the best thermal stability in pure IPA by showing a J–H transition at above 330 K, while in 88 mol% IPA, this temperature drops to about 320 K, and then at *ca.* 68 mol% IPA, only H-aggregates are formed at room temperature. Then, when the IPA content is lowered by about 9 mol%, the J-aggregate re-appears and its thermal stability improves with decreasing IPA content, till the J–H transition temperature

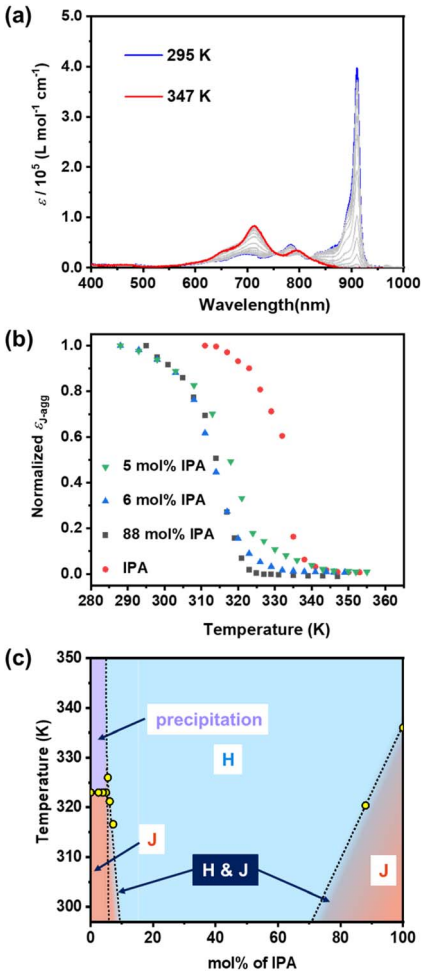

Fig. 4 (a) Absorption spectra of **1** (3.0×10^{-6} M) in mixed IPA (88 mol%) and water at varied temperatures; (b) extinction coefficient changes of the J-band with temperature exhibited by **1** (3.0×10^{-6} M) in different IPA–water mixtures, depicting the varied transition temperature between H- and J-aggregates in corresponding solvents; (c) schematic H–J thermal transition diagram of **1** (@ 3.0×10^{-6} M) in IPA–water solvents.

increases to above 320 K when IPA reaches *ca.* 5 mol% in water. As IPA drops to below 5 mol%, thermally induced precipitation occurs at about 323 K. This precipitation temperature remains roughly constant as the IPA content varies between 0 and 5 mol%. Presumably, such phenomena of thermally induced precipitation suggest that the J-aggregation process is favored by the entropy change in the low-IPA composition regime, similar to what happens in pure water. Since the entropy-driven mechanism only arises in highly water-rich solutions, it should be irrelevant to the J–H aggregate transition that takes place in solutions of higher IPA contents. These results not only indicate the enthalpy-driven nature of the H-to-J transition in solvents of 5 mol% IPA or more, they moreover reveal a nonlinear dependency of solvation properties on the solvent composition and underline the unusual behaviors of relevant IPA–water mixtures.

Subsequently, additional alcohols are investigated regarding the special solvation effects upon mixing with water. Basically, when introduced as a co-solvent to the aqueous solution of **1**, methanol, ethanol and *n*-propanol all exhibit similar ability in degrading the larger J-aggregates into smaller H-aggregates (Fig. 5 and S12†), although the specific component ranges that promote the H-type structures differ from one alcohol to another (Fig. 5). Compared with the IPA–H_2O system, *n*-propanol–H_2O shows a slightly wider H-aggregate range (*ca.* 6–83 mol% *n*-propanol), whereas ethanol displays a slightly contracted H-form span and methanol presents the narrowest H-region. Notably, these varied H-promoting composition widths, presumably reflecting the relative stability of the J-aggregate in respective binary systems, as well as the ability of different mixtures in solubilizing the amphiphiles and degrading the aggregates, do not at all concur with the thermal stability shown by the J-aggregates in respective pure alcohols (Fig. 2).

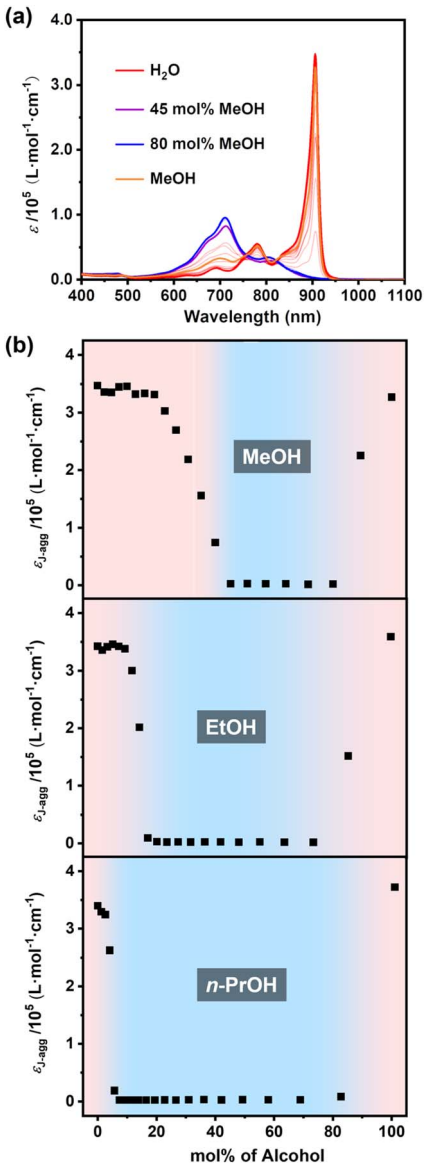

Fig. 5 (a) Absorption changes of **1** (3.0×10^{-6} M) in mixed MeOH–H_2O; (b) varied extinction coefficients of the J-band in binary solvents of methanol, ethanol and *n*-propanol mixed with water.

By comparing the H–J transition behaviours in the binary solvent systems of four different alcohols, it is wondered if reducing the size of the hydrocarbon moiety in alcohol molecules suppresses the H-formation, alternatively whether increasing the number of OH groups would entail similar effects. To test this hypothesis, ethylene glycol (EG) is inspected as a co-solvent (Fig. S14†). It is indeed found that when EG is mixed with water at any percentage, the solution of **1** invariably demonstrates the absorption characteristics of J-aggregates, without any spectral features of H-aggregation ever detected, even though EG itself is not a particularly favourable solvent for the J-aggregate, which is evidenced by the moderate J-band intensity depicted in pure EG. Apparently, the diol EG has better H-bonding ability, and it is thus suggested that the immiscibility of water with the aliphatic moiety in alcohol molecules might be responsible for the special solvation effect observed in the binary solvents composed of four mono-alcohols.

Finally, the aggregation behaviours of **2** are studied in binary solvents (Fig. S17†). As expected, because only H-aggregates are observed in the pure solvents of methanol, ethanol, *n*-propanol, and water at room temperature, J-aggregation is not observed in any of their binary mixtures. Moreover, as the J-aggregates of **2** possess only limited stability in IPA, unsurprisingly its H-aggregates readily take over when a minimal amount of water is added to the IPA solution. All these results reinforce the notion that hampered J-aggregation ability and more stabilized H-state result from steric congestion around the solvated side groups of the amphiphiles.

Molecular dynamics simulations

To enhance our comprehension of the relationship between water–alcohol mixtures featuring distinct mole ratios and molecular aggregates, a series of simulations were performed for different water–alcohol mixed solvents. Details of simulation are given in the ESI.† The dimerization energy of molecule **1** in IPA/methanol–water mixtures at varying mole ratios was computed and depicted in Fig. 6. The nonlinear trend implies a non-ideal interaction between the alcohol–water and solvent–solvate components in these two systems. In IPA–water, compound **1** exhibits dimerization energies of −138 and −108 kJ mol^{-1} in pure water and pure alcohol, respectively. As the alcohol–water mole ratios vary to 0.2, 0.4 and 0.7, the dimerization energy notably increases to −42, −39 and −63 kJ mol^{-1}, respectively.

A similar trend is observed for the water–methanol systems, which show dimerization energies of −138, −114, −105, −128 and −150 kJ mol^{-1} for methanol molar ratios of 0.0, 0.2, 0.4, 0.7, and 1.0, respectively. This result shows that the enthalpy-driven aggregation is weaker in mixed solvents than in two pure solvents. These findings are consistent with the experimental results, indicating that compound **1** exhibits a diminished propensity for aggregation within appropriately balanced water–alcohol mixtures, though the experiments actually demonstrate a partial dissociation of J-aggregates into smaller H-species under pertinent solvent conditions.

Assuming that the two solvents mutually influence each other's behaviours near the solute molecules, we simulated monomer **1** in water/IPA mixtures at several different molar ratios. We then calculated the normalized RDFs of each solvent

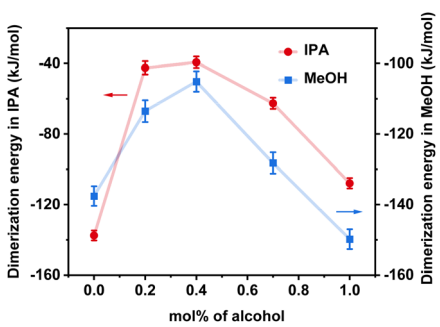

Fig. 6 Dimerization energy of **1** in water–IPA and water–methanol mixtures.

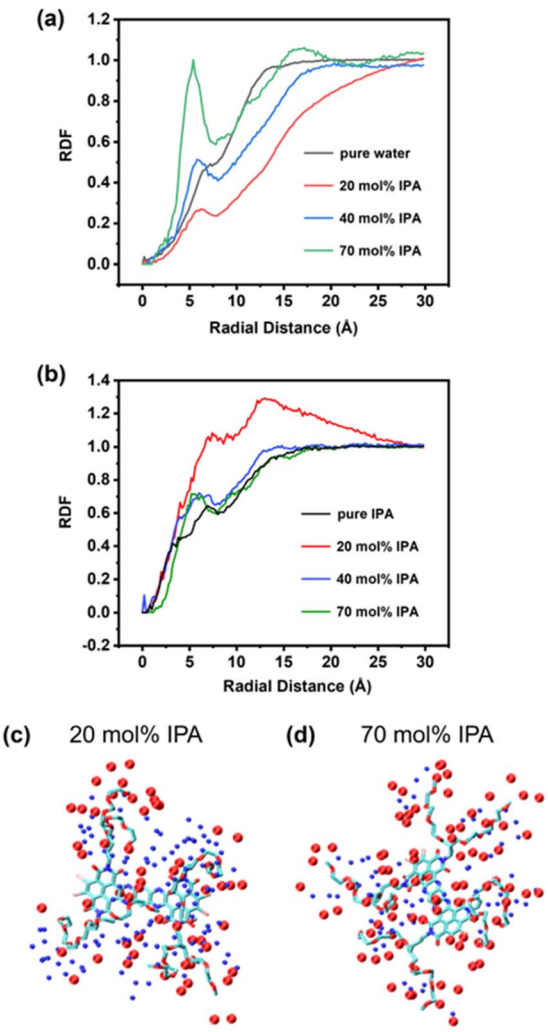

Fig. 7 RDF of centroid of water (a) and IPA (b) around molecule **1**; snapshots of solvent molecules (red beads representing IPA and blue beads representing water) within 5 Å of **1** with IPA at 20 mol% (c) and 70 mol% (d).

to compare their local enrichment around the solute molecules with their bulk concentrations (Fig. 7).

In both RDFs, the first peak defines the first solvation shell, which is 6–7 Å for water (Fig. 7a) and 5–8 Å for IPA (Fig. 7b). As the IPA fraction increases (Fig. 7a), the height of the water peak grows relative to the pure-water reference (black curve), reaching nearly twice the intensity at 70 mol% IPA. This result indicates that water–solute interactions are strengthened when water is the minor component. Conversely, in the 20 mol% IPA solution (red curve in Fig. 7b), IPA's local concentration around the solute is also enhanced despite its low bulk fraction. When both solvents are present in roughly equal proportions (40 mol% IPA; blue curves in Fig. 7a and b), we observe modest increases in the first-shell concentrations of both water and IPA.

These effects can be attributed to the weaker IPA–water interactions relative to solvent–solute interactions. As a result, the predominant bulk solvent "pushes" the minor component toward the solute, where water and IPA act cooperatively to form bridging networks around the solute's side chains (Fig. 7c and d). This mutual solvation enhancement reduces the driving force for aggregation as well as the size of the aggregates.

Discussion

From the experimental results, it is clear that the relative propensity of the J-aggregates for degradation in the binary solvent systems containing varied alcohols does not correlate with their thermodynamic stability in respective pure alcohols. This is evidenced by the disparate trends observed with the relative order of thermal dissociation temperature values exhibited by the J-aggregates in different alcohols (Fig. 2b), as compared to the widths of solvent composition ranges that promote H-aggregate formation in the binary solvent systems comprising respective alcohols (Fig. 1c). For example, while superior J-aggregate thermal stability with higher dissociation temperatures (indicating poor solvation and strengthened stacking of solute molecules) is manifested in IPA and *n*-propanol, wider composition ranges allowing H-aggregate formations (implying more easily disrupted J-aggregates) are detected with these two alcohols as well when mixed with water. The situations are just the opposite for ethanol and especially methanol. It is thus suggested that the unusual solvation behaviours are not highly dependent on the pure solvent properties of the alcohols. Hence, the J-to-H degradations and unique solvation abilities of pertinent binary media most likely arise from the solvent mixing process, instead of being inherent to either of the pure solvents. That is, the solvation mechanism of mixed water–alcohol media cannot be simply considered to be linearly added effects of two types of independent solvents. The enhanced solvation abilities are caused by a set of non-ideal behavioural patterns exhibited by water when interacting with various alcohol molecules, which are distinctively manifested by the current sophisticated trinary solute–solvent systems. Therefore, we subsequently looked up prior literature work focused on water–alcohol interactions.

Besides a volume of earlier reports on the thermodynamic properties of aqueous solutions,[42,49,50] more recently the microstructures of binary water–alcohol mixtures were studied with terahertz time-domain spectroscopy and pulsed field gradient NMR techniques.[47,51] A few important conclusions were drawn therein. First, within the low alcohol mole-fraction region, the hydration shell around the alcohol molecules increases with the size of the hydrophobic moiety of the alcohol molecule. Second, the extended hydrogen-bonded (H-bonded) networks formed between alcohol and water molecules reach the highest degree of structuring at about 30, 15, 10 and 10 mol% for methanol, ethanol, *n*-propanol and IPA, respectively. These values appear to agree semi-quantitatively with the solvent compositions, at which in our experiments the J-band starts to attenuate in respective alcohol–water mixtures. This finding further suggests that J-aggregate's degradation is related to the special microstructures of the water–alcohol mixtures. Presumably, the binary systems that exhibit higher degrees of structuring manifest enhanced solvation capacity. In particular, such highly structured H-bonded networks are more readily disrupted to accommodate the solvate (likely the triglyme side chains specifically), presumably by paying a lower energy penalty compared with the homogeneous pure solvents. This also explains why different alcohols enable H-aggregates at varied mole ratios in the mixtures. The alcohols having larger aliphatic groups feature thicker hydration shells, and therefore they can bring about the highly structured networks, required

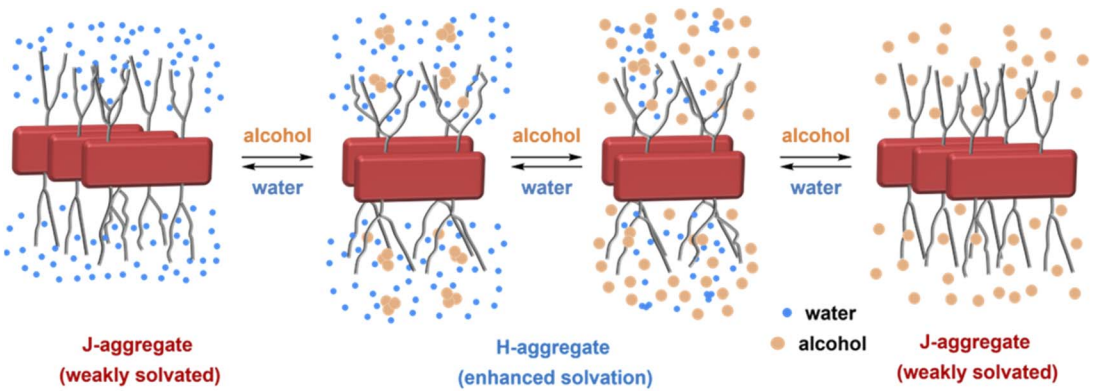

Fig. 8 Schematic representation of the J- and H-aggregate motif changes in binary solvents of varied compositions.

for degrading the J-aggregates more effectively at a lower mole ratio.

Conclusions

By examining the self-aggregation behaviors of a pair of amphiphilic aromatic polycycles in a series of binary solvents, the special solvation properties with unusual non-ideality effects are uncovered for water and low-carbon mono-alcohol mixtures. While molecule **1** assembles into long fibrous J-aggregates in pure water and different alcohols, H-aggregates with much lower degrees of association occur in binary water–alcohol solvents at medium mole ratios. That is, the mixed solvents degrade the supramolecular higher polymers into smaller oligomers, presumably by solvating this amphiphile more effectively than the respective pure solvents (Fig. 8). By virtue of the distinct spectral features of H- and J-aggregates, the exhibited supramolecular motif changes provide a convenient yet sensitive characterizing handle for the solvent properties. It is found that similar degradation processes commonly occur in binary solvents of various mono-alcohols, including methanol, ethanol, propanol, and isopropanol, but the H–J transition takes place at different volume ratios, depending on the alcohol structures. A wider composition range is observed with *n*-propanol–water mixtures for promoting the smaller H-aggregate formation, while methanol–water exhibits a narrower composition range favoring the H-aggregate. Moreover, such binary solvent-induced J–H transitions are shown to be driven by enthalpy changes, unlike the entropy-favored process in pure water, and they do not correlate with the thermal stability of J-aggregates in different pure alcohols. It is speculated that the enhanced solubilizing ability showing significant non-ideality is related to the special microscopic structural characteristics inherent to the pertinent water–alcohol mixtures.

Our experiments produce consistent results with those previously reported from a spectroscopic study, which uncovered that highly structured, H-bonded networks are formed by water–alcohol mixtures at certain mole ratios, and the current work further reveals that such structured media possess enhanced solvation ability and may induce degradation/dissociation of amphiphile aggregates. The solvation enhancement capacity varies with alcohol structures. Alcohols bearing larger hydrophobic groups, such as *n*- and *i*-propanol, feature thicker hydration shells, and they are thus capable of disrupting the aggregates more effectively at lower alcohol or water contents than alcohols with smaller alkyl groups. The work also demonstrates that supramolecular assemblies may be harnessed as useful molecular probes for interrogating the solvent properties and unveiling the sophisticated microstructures thereof.

Data availability

The data supporting this article have been included as part of the ESI.†

Author contributions

L. Meng, R. Wei, and D. Zhao conceptualized the project. D. Zhao and Y. Gao supervised the project. L. Meng and R. Wei synthesized the amphiphiles, performed experiments and related data analysis. Z. Xie performed the theoretical studies. D. Zhang contributed to the data fitting of dissociation curves and construction of the theoretical models. X. Wan participated in the synthesis work. H. Han and X. Xiao collected part of the NMR spectra and MS data. Z. Zhu and W. Shi collected the AFM images. The manuscript was written through the contributions of all authors.

Conflicts of interest

There are no conflicts to declare.

Acknowledgements

The work was financially supported by the National Natural Science Foundation of China (22431001, 22175004 and 21925501) and the Beijing National Laboratory for Molecular Sciences (BNLMS-CXXM-201902). The authors also acknowledge the Analytical Instrumentation Center of Peking University for the structural and spectral characterization. The computational resources were supplied by the High-performance Computing Platform of Peking University.

References

1 M. Hecht and F. Würthner, *Acc. Chem. Res.*, 2021, **54**, 642–653.
2 R. Ghosh and F. C. Spano, *Acc. Chem. Res.*, 2020, **53**, 2201–2211.
3 T. Aida, E. W. Meijer and S. I. Stupp, *Science*, 2012, **335**, 813–817.
4 L. Yang, X. Tan, Z. Wang and X. Zhang, *Chem. Rev.*, 2015, **115**, 7196–7239.
5 C. Ji, W. Cheng, Q. Yuan, K. Müllen and M. Yin, *Acc. Chem. Res.*, 2019, **52**, 2266–2277.
6 S. Xu, H.-W. Liu, S.-Y. Huan, L. Yuan and X.-B. Zhang, *Mater. Chem. Front.*, 2021, **5**, 1076–1089.
7 M. F. J. Mabesoone, A. R. A. Palmans and E. W. Meijer, *J. Am. Chem. Soc.*, 2020, **142**, 19781–19798.
8 F. Würthner, *J. Org. Chem.*, 2022, **87**, 1602–1615.
9 Q. Jin, L. Zhang and M. Liu, *Chem.–Eur. J.*, 2013, **19**, 9234–9241.
10 M. Ogasawara, X. Lin, H. Kurata, H. Ouchi, M. Yamauchi, T. Ohba, T. Kajitani, T. Fukushima, M. Numata, R. Nogami, B. Adhikari and S. Yagai, *Mater. Chem. Front.*, 2018, **2**, 171–179.
11 A. Isobe, D. D. Prabhu, S. Datta, T. Aizawa and S. Yagai, *Chem.–Eur. J.*, 2020, **26**, 8997–9004.
12 K. V. Rao and S. J. George, *Org. Lett.*, 2010, **12**, 2656–2659.
13 G. Ghosh and S. Ghosh, *Chem. Commun.*, 2018, **54**, 5720–5723.

14 G. Markiewicz, M. M. J. Smulders and A. R. Stefankiewicz, *Adv. Sci.*, 2019, **6**, 1900577.
15 J.-G. Jia, C.-C. Zhao, Y.-F. Wei, Z.-M. Zhai, S.-S. Bao, A. J. Jacobson, J. Ma and L.-M. Zheng, *J. Am. Chem. Soc.*, 2023, **145**, 23948–23962.
16 J. S. Valera, R. Gómez and L. Sánchez, *Small*, 2018, **14**, 1702437.
17 S. H. Jung, D. Bochicchio, G. M. Pavan, M. Takeuchi and K. Sugiyasu, *J. Am. Chem. Soc.*, 2018, **140**, 10570–10577.
18 A. Sarkar, R. Sasmal, C. Empereur-mot, D. Bochicchio, S. V. K. Kompella, K. Sharma, S. Dhiman, B. Sundaram, S. S. Agasti, G. M. Pavan and S. J. George, *J. Am. Chem. Soc.*, 2020, **142**, 7606–7617.
19 M. L. Ślęczkowski, M. F. J. Mabesoone, P. Ślęczkowski, A. R. A. Palmans and E. W. Meijer, *Nat. Chem.*, 2021, **13**, 200–207.
20 Z. Shen, Y. Jiang, T. Wang and M. Liu, *J. Am. Chem. Soc.*, 2015, **137**, 16109–16115.
21 T. Pal and D. Chaudhuri, *J. Am. Chem. Soc.*, 2023, **145**, 2532–2543.
22 P. A. Korevaar, C. Schaefer, T. F. A. de Greef and E. W. Meijer, *J. Am. Chem. Soc.*, 2012, **134**, 13482–13491.
23 Y. Lin, M. Penna, M. R. Thomas, J. P. Wojciechowski, V. Leonardo, Y. Wang, E. T. Pashuck, I. Yarovsky and M. M. Stevens, *ACS Nano*, 2019, **13**, 1900–1909.
24 Y. Chen, Q. Wan, Y. Shi, B. Tang, C.-M. Che and C. Liu, *Angew. Chem., Int. Ed.*, 2023, **62**, e202312844.
25 K. V. Rao, M. F. J. Mabesoone, D. Miyajima, A. Nihonyanagi, E. W. Meijer and T. Aida, *J. Am. Chem. Soc.*, 2020, **142**, 598–605.
26 A. Sarkar, T. Behera, R. Sasmal, R. Capelli, C. Empereur-mot, J. Mahato, S. S. Agasti, G. M. Pavan, A. Chowdhury and S. J. George, *J. Am. Chem. Soc.*, 2020, **142**, 11528–11539.
27 A. Nandakumar, Y. Ito and M. Ueda, *J. Am. Chem. Soc.*, 2020, **142**, 20994–21003.
28 E. Krieg, M. M. C. Bastings, P. Besenius and B. Rybtchinski, *Chem. Rev.*, 2016, **116**, 2414–2477.
29 Q. Wang, J. L. Mynar, M. Yoshida, E. Lee, M. Lee, K. Okuro, K. Kinbara and T. Aida, *Nature*, 2010, **463**, 339–343.
30 E. Cohen, H. Weissman, E. Shimoni, I. Kaplan-Ashiri, K. Werle, W. Wohlleben and B. Rybtchinski, *Angew. Chem., Int. Ed.*, 2017, **56**, 2203–2207.
31 V. Grande, B. Soberats, S. Herbst, V. Stepanenko and F. Würthner, *Chem. Sci.*, 2018, **9**, 6904–6911.
32 E. Krieg, A. Niazov-Elkan, E. Cohen, Y. Tsarfati and B. Rybtchinski, *Acc. Chem. Res.*, 2019, **52**, 2634–2646.
33 I. Helmers, B. Shen, K. K. Kartha, R. Q. Albuquerque, M. Lee and G. Fernández, *Angew. Chem., Int. Ed.*, 2020, **59**, 5675–5682.
34 I. Helmers, G. Ghosh, R. Q. Albuquerque and G. Fernández, *Angew. Chem., Int. Ed.*, 2021, **60**, 4368–4376.
35 Y. Tidhar, H. Weissman, S. G. Wolf, A. Gulino and B. Rybtchinski, *Chem.–Eur. J.*, 2011, **17**, 6068–6075.
36 B. Rybtchinski, *ACS Nano*, 2011, **5**, 6791–6818.
37 M. R. Molla and S. Ghosh, *Phys. Chem. Chem. Phys.*, 2014, **16**, 26672–26683.
38 P. P. N. Syamala and F. Würthner, *Chem.–Eur. J.*, 2020, **26**, 8426–8434.
39 P. P. N. Syamala, B. Soberats, D. Görl, S. Gekle and F. Würthner, *Chem. Sci.*, 2019, **10**, 9358–9366.
40 N. Bäumer, K. K. Kartha, J. P. Palakkal and G. Fernández, *Soft Matter*, 2020, **16**, 6834–6840.
41 M. García-Iglesias, M. J. Mayoral, D. Serrano-Molina, F. Aparicio, V. Vázquez-González and D. González-Rodríguez, *ChemPlusChem*, 2019, **84**, 488–492.
42 M. A. J. Gillissen, M. M. E. Koenigs, J. J. H. Spiering, J. A. J. M. Vekemans, A. R. A. Palmans, I. K. Voets and E. W. Meijer, *J. Am. Chem. Soc.*, 2014, **136**, 336–343.
43 S. Kotha, M. F. J. Mabesoone, D. Srideep, R. Sahu, S. K. Reddy and K. V. Rao, *Angew. Chem., Int. Ed.*, 2021, **60**, 5459–5466.
44 K. Cai, J. Xie and D. Zhao, *J. Am. Chem. Soc.*, 2014, **136**, 28–31.
45 K. Cai, J. Xie, D. Zhang, W. Shi, Q. Yan and D. Zhao, *J. Am. Chem. Soc.*, 2018, **140**, 5764–5773.
46 W. Shi, R. Wei, D. Zhang, L. Meng, J. Xie, K. Cai and D. Zhao, *Angew. Chem., Int. Ed.*, 2022, **61**, e202208635.
47 R. Li, C. D'Agostino, J. McGregor, M. D. Mantle, J. A. Zeitler and L. F. Gladden, *J. Phys. Chem. B*, 2014, **118**, 10156–10166.
48 X. Gao, W. Qiu, X. Yang, Y. Liu, Y. Wang, H. Zhang, T. Qi, Y. Liu, K. Lu, C. Du, Z. Shuai, G. Yu and D. Zhu, *Org. Lett.*, 2007, **9**, 3917–3920.
49 Y. M. Muñoz-Muñoz, G. Guevara-Carrion and J. Vrabec, *J. Phys. Chem. B*, 2018, **122**, 8718–8729.
50 F. Franks and D. J. G. Ives, *Q. Rev., Chem. Soc.*, 1966, **20**, 1–44.
51 W. S. Price, H. Ide and Y. Arata, *J. Phys. Chem. A*, 2003, **107**, 4784–4789.